applied sciences

MDPI

Article

Simulation and Experimental Assessment of the Usability of the Phase Angle Method of Examining the State of Shock Absorbers Installed in a Vehicle

Jacek Drobiszewski *, Zbigniew Lozia and Piotr Zdanowicz

Faculty of Transport, Warsaw University of Technology, ul. Koszykowa 75, 00-662 Warsaw, Poland; zbigniew.lozia@pw.edu.pl (Z.L.); piotr.zdanowicz@pw.edu.pl (P.Z.)
* Correspondence: jacek.drobiszewski@pw.edu.pl

Abstract: The technical condition of the shock absorbers used in automotive suspension systems is important with respect to vehicle occupants' comfort and traffic safety. Therefore, much effort has been made for many years to find diagnostic methods that would be more effective. There is a preference for those methods where the shock absorbers do not have to be dismounted from the vehicle. Among those being in use, the 'forced vibration methods' have earned the widest acceptance. One of them is the solution where the angle of phase shift between the vertical displacement of the vibration plate and the tyre–plate interaction force is measured. The authors decided to assess this method's usability by comparing simulation results with the results of experiments run on a prototype diagnostic test stand. They used two 'quarter-car' simulation models (linear and non-linear) and experimentally tested suspension systems of two medium-class cars. In the first stage, computations were made in the frequency domain for the linear model with two degrees of freedom, followed by simulations in the time domain, where an analogous but strongly non-linear model was used. In the latter model, the actual characteristic curves (determined during the laboratory measurements) of shock absorber damping, tyre and suspension elasticity, sliding friction in the suspension system, and tyre bouncing were taken into account. The authors have presented the computation results in the form of curves representing the phase angle as a function of the relative damping in the suspension system under test for the two medium-class cars. The suspensions of the cars had similar inertia properties but different characteristics of the spring and damping forces. The cars also differed from each other in the observed and measured level of the friction forces (twice bigger). The computation results obtained for the linear and non-linear model and the experiment results show a similar qualitative nature. In quantitative terms, however, they differ significantly from each other. The role of non-linearities is important. Nevertheless, the results show monotonicity and noticeable sensitivity to changes in the technical condition of the shock absorbers, which is an essential and desirable feature in diagnostics.

Keywords: phase shift; quarter car; experimental verification

Citation: Drobiszewski, J.; Lozia, Z.; Zdanowicz, P. Simulation and Experimental Assessment of the Usability of the Phase Angle Method of Examining the State of Shock Absorbers Installed in a Vehicle. *Appl. Sci.* **2024**, *14*, 10804. https://doi.org/10.3390/app142310804

Academic Editor: Suchao Xie

Received: 4 October 2024
Revised: 4 November 2024
Accepted: 19 November 2024
Published: 22 November 2024

1. Introduction

The vehicle ride comfort and running safety depend, inter alia, on the technical condition of the shock absorbers used in vehicle suspension systems [1–6]. With growing vehicles' time in service and mileage travelled, the effect of shock absorbers' functioning is weakening, and defects occur. Therefore, new, more effective methods of diagnosing their condition have been sought for many years [7–17]. In particular, the on-vehicle test methods are desirable because of the short time and low cost of the test. However, the present-day diagnostic equipment should be suitable for testing the shock absorbers that would be susceptible to changes in the temperature of the working fluid [18,19] and those of the controllable (e.g., magnetorheological [20]) type as well as the suspension systems with strong (and varying at that) sliding friction (e.g., in leaf springs [21]). The most modern

testers are also required to offer reliable results of the inspection of shock absorbers installed in unique vehicles with electric motors placed in wheel hubs [22], where the unsprung mass would be significantly increased because of that. Among the numerous methods used, the 'forced vibration methods' have earned the widest acceptance [3,7–17]. In such methods, the road wheel is forced to vibrate vertically with a frequency of 16–25 Hz, and then this frequency is lowered until the vibration disappears. Thus, the frequency range is 'swept', which includes the natural frequencies of the sprung and unsprung masses supported by the suspension springs and tyres as elastic elements. This method makes use of the widely known fact that the system vibration is highly sensitive to damping in the resonance zone. At present, the most popular solutions are the EUSAMA method [1,3,5,8–12,16,17,23–33] and its significantly modified version named the 'phase angle method' proposed by the Hunter company [16,17,24,28]. A somewhat less popular solution is the 'theta' method, where the suspension under test is assessed by means of a dimensionless damping coefficient (damping level), which is often denoted in the literature by symbol ϑ (or γ, β, D, etc.). There are a few variants of this method [7–9,11–14,29,30,32–34], which lead to an indirect assessment of the main damping element, i.e., the shock absorber. This method is analysed by the authors of this paper in other publications [3,25,33,35].

This article concerns the assessment of the usability of the phase angle method. In this solution (Figure 1), angle Φ_{ON} of the phase shift between excitation ζ (vertical displacement of the vibration plate) and force N at the contact between the road wheel (tyre) and the vibration plate [3,10,16,17,24,26,28,30,36,37] is measured. The authors decided to compare the results of a theoretical analysis based on simulations with the results of experimental tests carried out on a prototype diagnostic test stand.

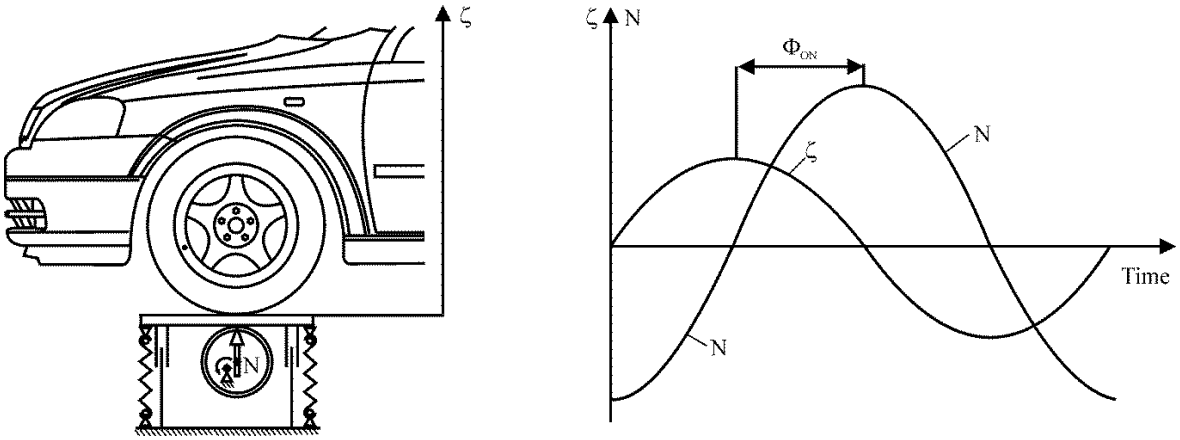

Figure 1. Illustration of the method of measuring angle Φ_{ON} of the phase shift between excitation ζ (vertical displacement of the vibration plate) and force N at the contact between the road wheel (tyre) and the vibration plate.

The authors were interested in whether, in the phase angle method (as opposed to the EUSAMA method), the results of the diagnostic test can be expected to be independent of the non-linearity of the tested system (in particular, friction in the suspension) and the disturbing effect of the inertia of the plate forcing the vibrations.

To do this, two 'quarter-car' models (linear and non-linear) were employed for the simulation, and two medium-class cars were used for the experimental tests. It was decided that, at first, the linear and non-linear models of the car placed on a diagnostic test stand (diagnostic tester) would be described, and only then the essence and properties of the phase angle method would be presented in detail. Such a sequence was chosen because it would be difficult to describe the method without using the notions presented in the description of the models.

2. Materials and Methods

2.1. Structure of the Linear Model Used in the Simulation Tests and Equations of Motion in the Time and Frequency Domains

As in publications [4,11,12,15–17,23,26,27,34,37–41], the linear 'quarter-car' model presented in Figure 2a was used (cf. with that in [20,28]). In Figure 2b, the inertia of the tester's vibration plate was taken into account after [17,27,34,35].

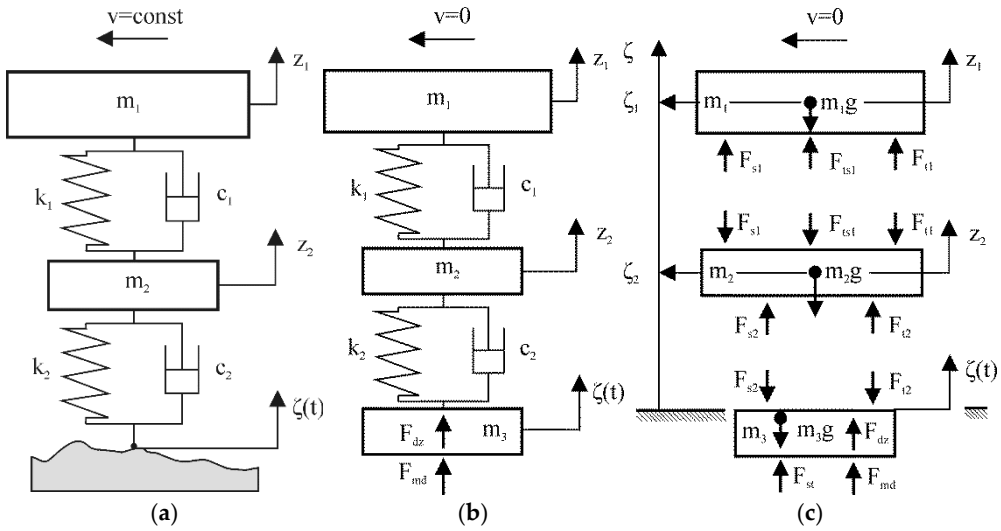

Figure 2. Schematic diagram of the 'quarter-car' model (for the notation, see the text): (**a**) general form of the linear model; (**b**) linear model for vehicle vibration testing on a diagnostic tester; (**c**) non-linear model for vehicle vibration testing on a diagnostic tester (with representation of the forces acting in the suspension and the tyre).

The model shown in Figure 2b consists of three mass elements, i.e., 'sprung mass' m_1 [kg], 'unsprung mass' m_2 [kg], and vibration plate m_3 [kg]. The suspension and tyre stiffness have been denoted by k_1 [N/m] and k_2 [N/m], respectively. Parameters c_1 [N·s/m] and c_2 [N·s/m] represent the suspension and tyre damping coefficients, respectively. The quantity denoted by $\zeta(t)$ [m] is the kinematic excitation resulting from the motion of the vibration plate (exciter), which supports the vehicle wheel. The measuring system measures the dynamic component F_{md} [N] of the force applied from below to the vibration plate, the static load N_{stm} resulting from the weight of the mass elements of the model (including the weight of the vibration plate $m_3 \cdot g$) and the force of inertia of the vibration plate F_{bp} (negative). The static forces are as follows:

$$N_{st} = (m_1 + m_2) \cdot g \tag{1}$$

$$N_{stm} = (m_1 + m_2 + m_3) \cdot g \tag{2}$$

The tyre–plate interaction force F_{op} [N] is equal to the sum of the static load N_{st} [N] and the dynamic component of the vertical force F_{dz} [N] in the tyre; the latter is equal to the sum of the dynamic spring force F_{dso} [N] (measured in relation to the state of static equilibrium, i.e., for the radial deformations of the tyre relative to the static deformation) and the force F_{two} [N] of viscous damping in the tyre:

$$F_{op} = F_{dz} + N_{st} \tag{3}$$

$$F_{dz} = F_{dso} + F_{two} \tag{4}$$

The diagnostic tester measures the force F_{opm} [N], which includes the dynamic component F_{md} [N] and the static reaction force N_{stm} [N] recorded at the beginning of the test.

The vibration plate's weight $m_3 \cdot g$ [N] and the force F_{bp} [N] of its inertia (negative) are also taken into account.

$$F_{opm} = F_{op} - F_{bp} + m_3 g = F_{op} + m_3 \frac{d^2\zeta(t)}{dt^2} + m_3 g = F_{dz} + N_{stm} + m_3 \frac{d^2\zeta(t)}{dt^2} = F_{md} + N_{stm} \quad (5)$$

$$F_{bp} = -m_3 \frac{d^2\zeta(t)}{dt^2} \quad (6)$$

$$F_{md} = F_{dz} + m_3 \frac{d^2\zeta(t)}{dt^2} \quad (7)$$

As mentioned above, F_{md} [N] is a result of the measurement of the dynamic component (where the static load N_{stm} [N] is not taken into account) of the force F_{dz} [N] in the tyre. The result of measurement of the force F_{dz} (i.e., the value of this force) and, in consequence, the value of force F_{op} as well, are distorted by the force of inertia F_{bp} [N] and weight $m_3 \cdot g$ [N] of the vibration plate. Moreover, the force F_{bp} introduces a phase shift of F_{md} in relation to F_{dz}. Figure 2b shows the vertical dynamic component F_{dz} of the tyre–plate interaction force (i.e., the dynamic component of the force in the tyre). This force is directed from the exciter plate to the tyre. The force F_{md}, i.e., the dynamic component of the vibration-exciting force generated in and measured by the diagnostic test stand, has also been indicated in the drawing.

The equations of motion for the linear model (Figure 2a) have been derived from the principle of dynamic force analysis. Their matrix form is represented by Equation (8), also showing the notation of individual matrices as follows: inertia—**M**; viscous damping—**C**; stiffness—**K**; the action of excitation through the damping in the tyre—$\mathbf{C}_\zeta$; the action of excitation through tyre's radial stiffness—$\mathbf{K}_\zeta$. The vectors of generalised coordinates (displacements), velocities, and accelerations have been denoted by $\mathbf{q}$, $\dot{\mathbf{q}}$, $\ddot{\mathbf{q}}$, respectively. The said notation has been used to write the equations of motion in a concise form (9).

$$\underbrace{\begin{bmatrix} m_1 & 0 \\ 0 & m_2 \end{bmatrix}}_{\mathbf{M}} \cdot \underbrace{\begin{bmatrix} \ddot{z}_1 \\ \ddot{z}_2 \end{bmatrix}}_{\ddot{\mathbf{q}}} + \underbrace{\begin{bmatrix} c_1 & -c_1 \\ -c_1 & c_1 + c_2 \end{bmatrix}}_{\mathbf{C}} \cdot \underbrace{\begin{bmatrix} \dot{z}_1 \\ \dot{z}_2 \end{bmatrix}}_{\dot{\mathbf{q}}} + \underbrace{\begin{bmatrix} k_1 & -k_1 \\ -k_1 & k_1 + k_2 \end{bmatrix}}_{\mathbf{K}} \cdot \underbrace{\begin{bmatrix} z_1 \\ z_2 \end{bmatrix}}_{\mathbf{q}} = \underbrace{\begin{bmatrix} 0 \\ c_2 \end{bmatrix}}_{\mathbf{C}_\zeta} \cdot \dot{\zeta} + \underbrace{\begin{bmatrix} 0 \\ k_2 \end{bmatrix}}_{\mathbf{K}_\zeta} \cdot \zeta \quad (8)$$

$$\mathbf{M} \cdot \ddot{\mathbf{q}} + \mathbf{C} \cdot \dot{\mathbf{q}} + \mathbf{K} \cdot \mathbf{q} = \mathbf{C}_\zeta \cdot \dot{\zeta} + \mathbf{K}_\zeta \cdot \zeta \quad (9)$$

At the next stage, the Laplace transform of Equation (9) was determined for zero initial conditions. The solution obtained after appropriate transformations has the form shown in Equation (10), where the domain $s = r + i \cdot \omega$ has a real part r and an imaginary part ω (where $i^2 = -1$ and ω is radian frequency [rad/s]).

$$\mathbf{q}(s) = \mathbf{H}_\mathbf{q}(s) \cdot \zeta(s) \quad (10)$$

The operator transmittances (transfer functions) for displacements $\mathbf{H}_\mathbf{q}(\mathbf{s})$, velocities, and accelerations have been shown as Equations (11), (12), and (13), respectively.

$$\mathbf{H}_\mathbf{q}(\mathbf{s}) = \begin{bmatrix} H_{q_1}(s) \\ H_{q_2}(s) \end{bmatrix} = \frac{\mathbf{q}(\mathbf{s})}{\zeta(s)} = (\mathbf{M} \cdot s^2 + \mathbf{C} \cdot s + \mathbf{K})^{-1} \cdot (\mathbf{C}_\zeta \cdot s + \mathbf{K}_\zeta) \quad (11)$$

$$\mathbf{H}_{\dot{\mathbf{q}}}(s) = \begin{bmatrix} H_{\dot{q}_1}(s) \\ H_{\dot{q}_2}(s) \end{bmatrix} = \frac{\dot{\mathbf{q}}(\mathbf{s})}{\zeta(s)} = s \cdot \mathbf{H}_\mathbf{q}(\mathbf{s}) \quad (12)$$

$$\mathbf{H}_{\ddot{\mathbf{q}}}(s) = \begin{bmatrix} H_{\ddot{q}_1}(s) \\ H_{\ddot{q}_2}(s) \end{bmatrix} = \frac{\ddot{\mathbf{q}}(\mathbf{s})}{\zeta(s)} = s^2 \cdot \mathbf{H}_\mathbf{q}(\mathbf{s}) \quad (13)$$

The linear model describes changes in the dynamic components F_{dz} and F_{md} of the forces under analysis (Equations (4) and (7), measured as relative to the values observed in

the static equilibrium conditions. The total values of the tyre–plate interaction force F_{op} and the force F_{opm} measured in the test stand are described by Equations (3) and (5). They differ from the dynamic component values F_{dz} and F_{md} in the constant weight values of the model's mass elements (N_{st} and N_{stm}, respectively, according to (1) and (2)).

The Laplace transform of the dynamic vertical tyre–plate interaction force is expressed by Formula (14).

$$F_{dz}(s) = c_2 \cdot [\dot{\zeta}(s) - \dot{z}_2(s)] + k_2 \cdot [\zeta(s) - z_2(s)] \tag{14}$$

On the grounds of Equations (10)–(14), with necessary transformations, the final concise form (15) of the transmittance of the dynamic vertical tyre–plate interaction force was obtained (remembering that $q_1 = z_1$, $q_2 = z_2$):

$$H_{Fdz}(s) = \frac{F_{dz}(s)}{\zeta(s)} = (c_2 \cdot s + k_2) \cdot \left[1 - H_{q_2}(s)\right] \tag{15}$$

The difference between the dynamic component F_{md} of the force measured in the test facility and the vertical dynamic component F_{dz} of the tyre–plate interaction force is caused by the force of inertia of the plate (the last summand in (16)).

$$\begin{aligned} H_{Fmd}(s) &= \frac{F_{md}(s)}{\zeta(s)} = \frac{F_{dz}(s) + m_3 \cdot \ddot{\zeta}(s)}{\zeta(s)} = \frac{F_{dz}(s) + m_3 \cdot s^2 \cdot \zeta(s)}{\zeta(s)} = \\ &= (c_2 \cdot s + k_2) \cdot \left[1 - H_{q_2}(s)\right] + m_3 \cdot s^2 = H_{Fdz}(s) + m_3 \cdot s^2 \end{aligned} \tag{16}$$

The values of spectral transmittances $H_{Fdz}(i \cdot \omega)$ and $H_{Fmd}(i \cdot \omega)$, where ω is the radian frequency of kinematic excitation ζ, are defined for $s = i \cdot \omega$. Their moduli are equal to the ratios of the amplitudes of forces (F_{dz} and F_{md}, as appropriate) to the amplitude of excitation ζ, and the arguments are defined by the phase shifts.

By comparing the moduli of the transmittances H_{Fdz} and H_{Fmd} with each other (for identical excitation), it will be possible to assess indirectly the impact of mass m_3 of the tester's vibration plate on the differences between forces F_{dz} i F_{md}.

In their publications [27,35], the authors have presented the formulas that define the natural radian and Hertz frequencies of the undamped system (resonance radian frequencies ω_{01}, ω_{02} [rad/s] and Hertz frequencies f_{01}, f_{02} [Hz]) as well as suspension's critical damping c_{kr1} [N·s/m] and relative damping ϑ_1 [-].

$$\omega_{01/02}^2 = \frac{k_1 \cdot m_2 + (k_1 + k_2) \cdot m_1}{2 \cdot m_1 \cdot m_2} \mp \sqrt{\left[\frac{k_1 \cdot m_2 + (k_1 + k_2) \cdot m_1}{2 \cdot m_1 \cdot m_2}\right]^2 - \frac{k_1 \cdot k_2}{m_1 \cdot m_2}} = (2\pi \cdot f_{01/02})^2 \tag{17}$$

$$c_{kr1} = 2 \cdot \sqrt{\frac{k_1 \cdot k_2 \cdot m_1}{k_2 + k_1 \cdot \left(1 + \frac{m_2}{m_1}\right)}} \approx 2 \cdot \sqrt{\frac{k_1 \cdot k_2 \cdot m_1}{k_2 + k_1}} \text{ for } m_1 \gg m_2 \tag{18}$$

$$\vartheta_1 = \frac{c_1}{c_{kr1}} \tag{19}$$

where c_1 [N·s/m] is the viscous damping coefficient of the suspension system in the linear model defined previously.

2.2. Structure of the Non-Linear Model Used in the Simulation Tests and Its Equations of Motion in the Time Domain

The structure of the non-linear 'quarter-car' model (Figure 2c) is similar to that of the linear one (see also [3,5,35]). It differs from the latter in the description of the spring and damping forces in the suspension system and pneumatic tyre. It reflects the actual characteristic curves measured in laboratory conditions and represents shock absorber and tyre damping forces F_{t1} [N] and F_{t2} [N], respectively, suspension and tyre spring forces Fs_1 [N] and Fs_2 [N], respectively, sliding friction in the suspension Fts_1 [N], and tyre bouncing ('wheel hop') phenomenon. The non-linear model describes changes in the resultant forces F_{op} and F_{opm}, taking into account the constant values of the gravity forces of the model

masses (N_{st} and N_{stm}, respectively, according to Equations (1) and (2)). For the positions of the extremes of the curves under analysis relative to each other to be described (in terms of both the time and phase of the process), the dynamic components of the said resultant forces are important. Therefore, the authors focused mainly on forces F_{dz} and F_{md} (see Figure 2b,c and Formulas (4) and (7)).

Relation (20) presents the equations of motion of the non-linear 'quarter-car' model. The equations have also been derived from the principle of dynamic force analysis.

$$\begin{cases} \ddot{\zeta}_1 = \frac{Fs_1+Fts_1+Ft_1}{m_1} - g \\ \ddot{\zeta}_2 = \frac{-Fs_1-Fts_1-Ft_1+Fs_2+Ft_2}{m_2} - g \end{cases} \tag{20}$$

where $\ddot{\zeta}_1$ and $\ddot{\zeta}_2$ are accelerations of the sprung and unsprung mass, respectively; Fs_1, Fts_1, and Ft_1 are forces of elasticity, sliding friction, and viscous damping in the suspension system, respectively; Fs_2 and Ft_2 are tyre spring and damping (substitute viscotic) forces, respectively; and g is gravitational acceleration.

The spring force in the suspension (21) was approximated by a linear function and a third-degree polynomial.

$$Fs_1 = \begin{cases} A1s_1 \cdot u_1 & \text{for } u_1 \le u_{1gr} \\ A2s_1 \cdot u_1^3 + B2s_1 \cdot u_1^2 + C2s_1 \cdot u_1 + D2s_1 & \text{for } u_1 > u_{1gr} \end{cases} \tag{21}$$

where $A1s_1$ and $A2s_1$ through $D2s_1$ are coefficients of the functions that describe (as appropriate) the force of suspension elasticity at small and large deflections, respectively; u_{1gr} is the threshold of applicability of different formulas describing the spring force; u_1 is the suspension deflection defined by Formula (22).

$$u_1 = \zeta_2 - \zeta_1 + om_0 \tag{22}$$

where om_0 is the difference between coordinates ζ_1 and ζ_2, corresponding to $Fs_1 = 0$.

The sliding friction force in the suspension has been expressed by Equation (23).

$$Fts_1 = \begin{cases} Ats_1 \cdot sgn\dot{u}_1 & \text{for} \left|\dot{u}_1\right| > \dot{u}_{1gr} \\ Ats_1 \cdot \frac{\dot{u}_1}{\dot{u}_{1gr}} & \text{for} \left|\dot{u}_1\right| \le \dot{u}_{1gr} \end{cases} \tag{23}$$

where Ats_1 is the amplitude of the sliding friction force in the suspension system; $\dot{u}_{1gr}$ is the threshold value of velocity $\dot{u}_1$ of the suspension deflection, according to (24).

$$\dot{u}_1 = \dot{\zeta}_2 - \dot{\zeta}_1 \tag{24}$$

The viscous damping force in the suspension has been expressed by Equation (25).

$$Ft_1 = \begin{cases} -i_z \cdot c_o \cdot \left(-\dot{u}_1 \cdot i_z\right)^{Wo} & \text{for } \dot{u}_1 < 0 \\ i_z \cdot c_u \cdot \left(\dot{u}_1 \cdot i_z\right)^{Wu} & \text{for } \dot{u}_1 \ge 0 \end{cases} \tag{25}$$

where i_z is a coefficient that describes the kinematic relations in the suspension; c_o and c_u are coefficients of rebound and compression damping in the shock absorber, respectively; Wo and Wu are exponents of the functions describing the rebound and compression damping in the shock absorber, respectively.

The spring force in the pneumatic tyre was approximated by a third-degree polynomial (26).

$$Fs_2 = As_2 \cdot u_2^3 + Bs_2 \cdot u_2^2 + Cs_2 \cdot u_2 \tag{26}$$

where As_2 through Cs_2 are coefficients of the polynomial describing the spring force in the pneumatic tyre, and u_2 is the radial deflection of the tyre as defined in (27).

$$u_2 = \begin{cases} \zeta - \zeta_2 + R & \text{for } \zeta - \zeta_2 + R \geq 0 \\ 0 & \text{for } \zeta - \zeta_2 + R < 0 \end{cases} \quad (27)$$

where R is the free radius of the tyre.

According to (28), the tyre damping force is represented in the tyre model as a linear function of the velocity of radial deflection of the tyre.

$$Ft_2 = c_2 \cdot \dot{u}_2 \quad (28)$$

where c_2 is the coefficient of damping and $\dot{u}_2$ is the velocity of deflection as defined in (29).

$$\dot{u}_2 = \begin{cases} \dot{\zeta} - \dot{\zeta}_2 & \text{for } \zeta - \zeta_2 + R \geq 0 \\ 0 & \text{for } \zeta - \zeta_2 + R < 0 \end{cases} \quad (29)$$

The equations of motion (20) were solved in the time domain by means of approximate techniques with numerical integration using an authorial program developed in the Matlab-Simulink environment.

2.3. Parameters of the Linear and Non-Linear Model

The simulation calculations were carried out for the 'quarter-car' model data corresponding to rear suspension systems of medium-class passenger cars Opel Astra Van (segment C of the market) and Opel Agila (segment VAN micro of the market). The data for the linear and non-linear models of both vehicles have been summarised in Tables 1–4. The data also include specifications of the diagnostic tester used in the experiments; the data will be described hereafter.

The values of parameters of the non-linear model correspond to the results of laboratory measurements carried out on real objects. There is adequate conformity between geometric and mass parameters, as well as spring and damping characteristics of the suspension system (inclusive of the sliding friction forces) and of the tyre. The suspension damping coefficient c1 in the linear model stems from the assumption made that the value of energy dissipated during a single cycle in the linear symmetric shock absorber being simulated (Figure 2a,b) is equal to that in the real non-linear shock absorber. The c_1 value thus determined is taken as a basis for determining the relative suspension damping ϑ_1 (see (19)). The sliding friction force Fts_1 is not taken into account in the linear model. This means that ϑ_1 represents the damping of the shock absorber alone instead of the total damping of the complete car's suspension system.

Table 1. Parameters of the linear model of the rear 'quarter' of the Opel Astra car.

Symbol	Unit of Measure	Value
m_1	kg	160
m_2	kg	35
k_1	N/m	24,882
k_2	N/m	206,526
c_2	N·s/m	150
f_{01} (ω_{01})	Hz (rad/s)	1.87 (11.77)
f_{02} (ω_{02})	Hz (rad/s)	12.96 (81.42)
c_{kr1}	N·s/m	3770

Table 2. Additional parameters of the non-linear model of the rear 'quarter' of the Opel Astra car and of the diagnostic tester.

Symbol	Unit of Measure	Value
$A1s_1$	N/m	4.400×10^5
$A2s_1$	N/m^3	7.290×10^5
$B2s_1$	N/m^2	-5.037×10^4
$C2s_1$	N/m	2.155×10^4
$D2s_1$	N	4.094×10^2
u_{1gr}	m	0.001
om_0	m	0.309
Ats_1	N	40
$\dot{u}_{1gr}$	m/s	0.005
c_u	$N{\cdot}s^{Wu}/m^{Wu}$	14,000 *
c_o	$N{\cdot}s^{Wo}/m^{Wo}$	6700 *
Wu	-	1.9 *
Wo	-	1.6 *
i	-	0.7068
As_2	N/m^3	-3.021×10^7
Bs_2	N/m^2	3.592×10^6
Cs_2	N/m	1.553×10^5
R	m	0.311
m_3	kg	14.5
ζ_{min}	m	0.000
ζ_{max}	m	0.006

* Values for the experimental (adjustable) viscous damper set to '19' ($\vartheta_1 = 0.496$); lower damping levels were obtained by multiplying the damping force (described by a power function) in succession by 0.26; 0.30; 0.34; 0.41; 0.49; 0.62; and 0.78 so as to represent the damping curves of the experimental viscous damper for its settings being changed in succession from '12' to '18' ($\vartheta_1 = 0.131$; $\vartheta_1 = 0.155$; $\vartheta_1 = 0.173$; $\vartheta_1 = 0.207$; $\vartheta_1 = 0.242$; $\vartheta_1 = 0.300$; $\vartheta_1 = 0.366$).

Table 3. Parameters of the linear model of the rear 'quarter' of the Opel Agila car.

Symbol	Unit of Measure	Value
m_1	kg	167
m_2	kg	28
k_1	N/m	24,887
k_2	N/m	186,857
c_2	N·s/m	150
f_{01} (ω_{01})	Hz (rad/s)	1.82 (11.45)
f_{02} (ω_{02})	Hz (rad/s)	13.86 (87.06)
c_{kr1}	N·s/m	3826

Table 4. Additional parameters of the non-linear model of the rear 'quarter' of the Opel Agila car and of the diagnostic tester.

Symbol	Unit of Measure	Value
$A1s_1$	N/m	450,000
$A2s_1$	N/m^3	0
$B2s_1$	N/m^2	0
$C2s_1$	N/m	24,887
$D2s_1$	N	425
u_{1gr}	m	0.001
om_0	m	0.339
Ats_1	N	20
$\dot{u}_{1gr}$	m/s	0.005
c_u	$N{\cdot}s^{Wu}/m^{Wu}$	5600 *
c_o	$N{\cdot}s^{Wo}/m^{Wo}$	4500 *

Table 4. *Cont.*

Symbol	Unit of Measure	Value
Wu	-	1.5 *
Wo	-	1.5 *
i	-	0.86
As_2	N/m^3	0
Bs_2	N/m^2	1,584,000
Cs_2	N/m	149,000
R	m	0.279
m_3	kg	14.5
ζ_{min}	m	0.000
ζ_{max}	m	0.006

* Values for the experimental (adjustable) viscous damper set to '18' ($\vartheta_1 = 0.396$); lower damping levels were obtained by multiplying the damping force (described by a power function) in succession by 0.12; 0.13; 0.145; 0.155; 0.17; 0.185; 0.2; 0.22; 0.24; 0.27 0.3; 0.33; 0.39; 0.44; 0.52; 0.63; and 0.79 so as to represent the damping curves of the experimental viscous damper for its settings being changed in succession from '1' to '17' ($\vartheta_1 = 0.055$; $\vartheta_1 = 0.06$; $\vartheta_1 = 0.066$; $\vartheta_1 = 0.071$; $\vartheta_1 = 0.078$; $\vartheta_1 = 0.085$; $\vartheta_1 = 0.092$; $\vartheta_1 = 0.1$; $\vartheta_1 = 0.109$; $\vartheta_1 = 0.12$; $\vartheta_1 = 0.134$; $\vartheta_1 = 0.15$; $\vartheta_1 = 0.171$; $\vartheta_1 = 0.195$; $\vartheta_1 = 0.224$; $\vartheta_1 = 0.267$; $\vartheta_1 = 0.324$); for the higher damping level (set to '19'), in turn, a multiplier '1.39' was used (and obtained $\vartheta_1 = 0.514$).

3. Results

3.1. Experimental Tests on a Prototype Diagnostic Tester

To carry out the experimental tests, a prototype TUZ-1/E diagnostic test stand made by UNIMETAL was used, which was a modified EUSAMA diagnostic device with a constant amplitude of 3 mm of the sinusoidal excitation $\zeta(t)$ (see Tables 2 and 4). The device is equipped with an embedded microprocessor measurement system that can measure the force F_{md} (Figure 2b,c), vertical displacement and acceleration of the exciter plate. The stand is equipped with two strain gauge sensors for the force under each plate, a laser displacement sensor, and a MEMS acceleration sensor for the plate.

A summary of the sensors used is included in Table 5.

Table 5. Specification test stand sensors.

Measured Value	Sensor Type	Range	Accuracy
Force	Strain Gauge UNIMETAL, Złotów, Poland	±30 kN	0.1%
Displacement	Laser Panasonic HL-G105	±0.01 m	0.1%
Acceleration	MEMS TE Connectivity 4312M3-10	±10 g	0.5%

Thanks to the fact that the time histories of the accelerations were known, the impact of the exciter's inertia on the test results could be analysed. During the tests, time histories of the excitation ζ, its second derivative ($d^2\zeta(t)/dt^2$), as well as force F_{opm} (and, in consequence, force F_{md}), were simultaneously recorded. Thanks to that, the current values of the phase angle of the quantities under analysis and the phase shift between them could be calculated as well.

In the vehicles' rear suspension systems under test, special (experimental) shock absorbers with adjustable damping were used (Figure 3). We used an adjustable viscous damper of the structure described in [42]. Their damping curves were reduced to the direction of operation of the vehicle's suspension ζ_1, ζ_2 (see Figure 2c). Particular attention was paid to low values of the relative damping because they occur when the shock absorbers are in poor technical condition. This is important from the point of view of diagnostic tests. The other vehicle parameters were not changed, and their values were set at the nominal level.

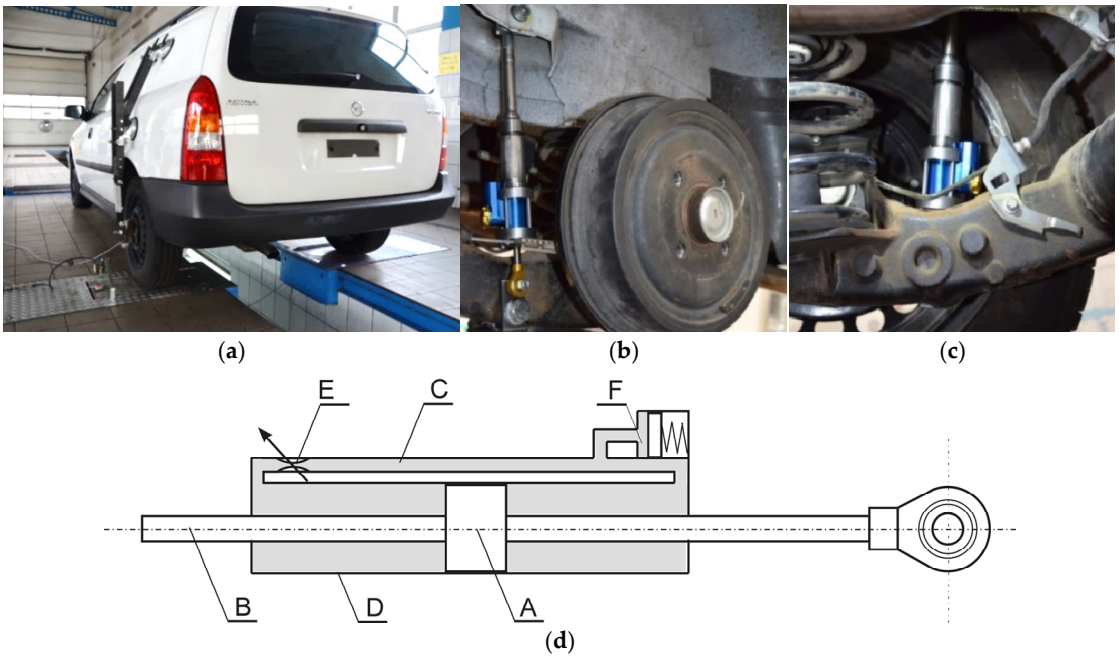

Figure 3. General view and details of the vehicle under test: (**a**) general view of the vehicle placed on the diagnostic stand during tests; (**b**) view of the adjustable viscous damper in the rear suspension system (from outside, with the vehicle wheel dismounted); (**c**) view of the adjustable viscous damper in the rear suspension system (from inside); (**d**) structure of the adjustable damper (base on [42]); A—piston, B—piston rod, C—bypass channel, D—damper body, E—adjustable throttle valve, F—compensation chamber.

3.2. Description of the Phase Angle Method and of the Proposed Necessary Correction to the Interpretation of the Test Results

The phase angle method has been proposed in a patent (see [17]) and in publication [16]. In publications [16,24,28,37], the authors gave its assessment, taking into account the disturbances encountered in real vehicle operation. The quantity that is analysed in this method (Figure 1) is the phase shift angle Φ_{ON} [rad] or [deg] (hereafter also referred to as 'phase angle') between the excitation ζ [m] (vertical displacement of the vibration plate of the diagnostic test stand) and the contact force N [N] between the tyre and the vibration plate. Figure 2b illustrates important elements to understand the physical sense of the phase angle Φ_{ON}. In the description of the patent [17], it has been mentioned that the impact of the vibration plate's inertia is taken into account in the process of determining force N.

Some weak points of this method have been discovered by other authors and mentioned in their publications [16,30,37]. They include high sensibility to changes in the tyre's radial stiffness (k_2), which significantly depends on the tyre inflation pressure [16,30,37], and to changes in the unsprung mass (m_2), resulting from tyre wear or wheel rim replacement (e.g., replacement of steel rims with ones made of light alloys) [16,37]. The disturbing impact of changes in the sprung mass (m_1) and suspension stiffness (k_1) has also been noticed [16,37].

In publications [16,17,24,28,37], however, the results have been presented in the $<0, \pi>$ range and have another form, i.e., they are a mirror reflection in relation to a horizontal line on a level of π. To avoid the said difficulties with the interpretation and presentation of the results, the author of the publication [26] has proposed a procedure as follows. φ angle is the result of the analysis of real and imagined parts of transmittance $H_{Fdz}(i\cdot\omega)$ or $H_{Fdzm}(i\cdot\omega)$. This reduces phase angle to range $<0, 2\pi>$ instead of $<-\pi/2, \pi/2>$ when

using the arctangent function. According to the definition of Φ_{ON} provided in [16,25], the following relations exist (details in [26]):

$$\Phi_{ON} = 2 \cdot \pi - \varphi = \Phi + \pi \tag{30}$$

To avoid the introduction of a new interpretation of this angle, the author of [26] has proposed, in the case of employing the phase angle method, to perform two transformations (in the interpretation consistent with publications [16,24,37]). The first one consists of changing the sense of force N to $N_T = -N$. The other transformation is expressed by Equation (31), which is a shortened form of Equation (30).

$$\Phi = \pi - \varphi = \Phi_{ON} - \pi \tag{31}$$

Thus, Figure 4 is generated to present angle Φ. This angle correctly corresponds, in both qualitative and quantitative terms, to the verbal definition of the phase shift angle Φ_{ON} in publications [16,24,37], but its geometric interpretation is different (Figure 4).

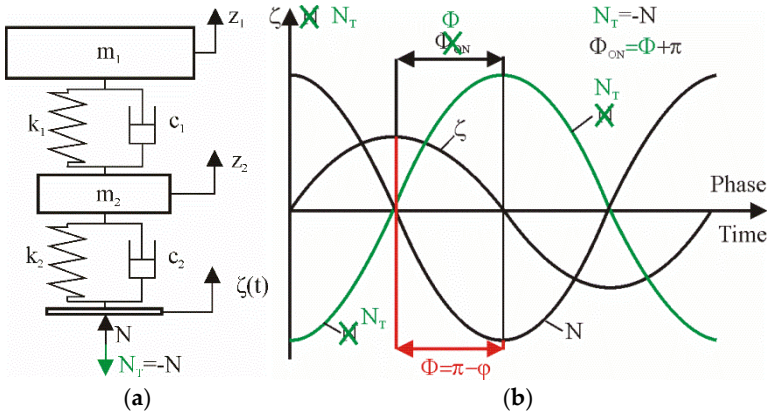

Figure 4. Proposal of a modification to the model and a change in the interpretation of the phase angle with reference to publications [16,24,37]: (**a**) modified 'quarter-car' model; (**b**) new way of interpretation of the simulation results obtained in the time domain (ζ(t)—excitation; $N_T(t) = -N(t)$, i.e., the vertical contact force between the tyre and the tester's vibration plate).

Figure 5 shows the calculation results obtained for the rear suspension system of a medium-class passenger car, Opel Astra Van. The graphs represent the phase shift angle Φ (also referred to in short as 'phase angle') as a function of excitation frequency f for various levels of relative suspension damping ϑ_1 ('Theta1' in the drawing). Figure 5a shows the values of the phase shift angle Φ(f) ('Fi' in the drawing) for the system response measured as the contact force between the tyre and the tester's vibration plate. Figure 5b shows, in turn, the curves that represent the said angle, denoted here by Φ_m(f) ('Fim' in the drawing), for the system response understood as the force measured in the test stand (and including the disturbing impact of the inertia of the vibration plate). The black dots indicate the minimums of the curves representing the said angle. With growing values of the relative suspension damping coefficient ϑ_1 ('Theta1'), the minimum values of the phase shift angle are increasing as well, occurring within the frequency range of 4–14 Hz. These minimums occur for frequencies decreasing with growing relative damping ϑ_1 ('Theta1').

Figure 6 shows the simulation results obtained for the non-linear 'quarter-car' model, and the results of measurements carried out on the prototype test stand TUZ-1/E for the rear suspension system of the Opel Astra Van car. Figure 6a shows the curves that represent the phase angle as a function of the frequency of the contact force between the tyre and the vibration plate (without the disturbing impact of the inertia of the vibration plate), and Figure 6b shows analogous test results but obtained for the force measured in the test stand (and including the disturbing impact of the inertia of the vibration plate). In this case, the

relative damping coefficient was $\vartheta_1 = 0.242$. The black dots indicate the minimums of the curves representing the phase shift angle.

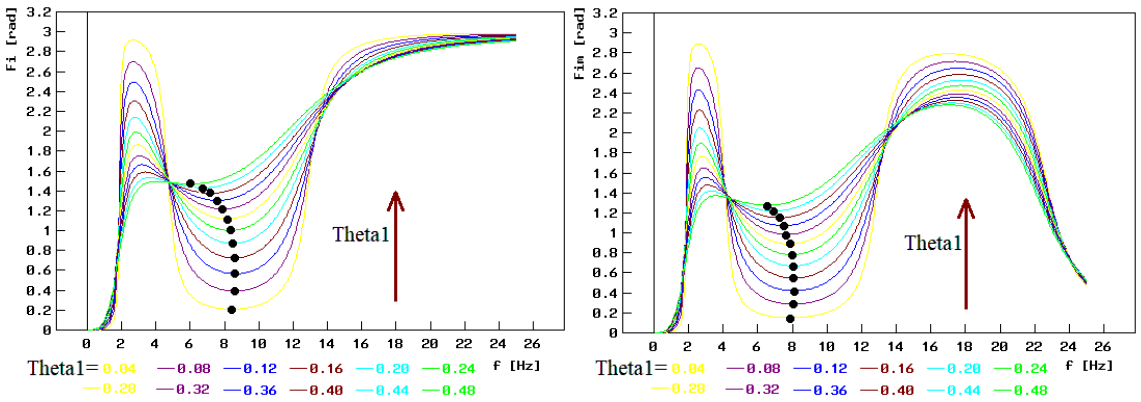

Figure 5. Phase angle vs. frequency curves for various levels of relative suspension damping ϑ_1 ('Theta1' in the drawing) in the rear suspension system of the Opel Astra Van car (the dots indicate the minimum values): (**a**) values of Φ(f) ('Fi' in the drawing) for the response understood as the force between the tyre and the vibration plate; (**b**) values of Φ_m(f) ('Fim' in the drawing) for the response understood as the force measured in the test stand.

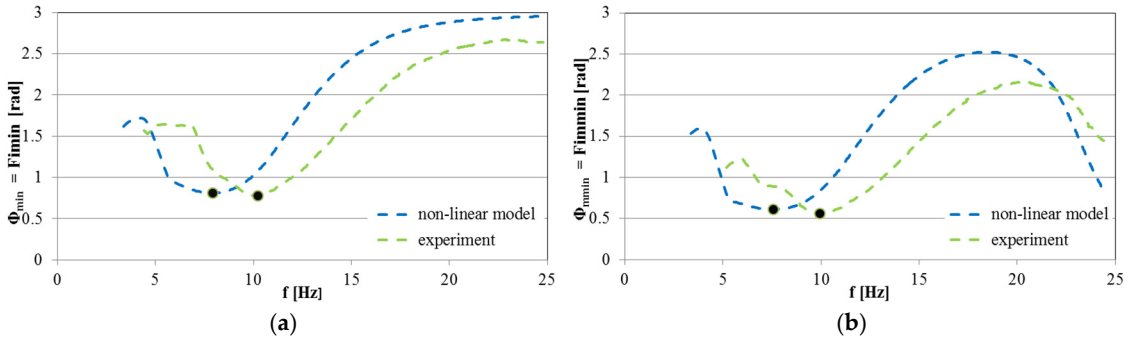

Figure 6. Simulation results obtained for the non-linear 'quarter-car' model and results of measurements carried out on the prototype test stand TUZ-1/E for the rear suspension system of the Opel Astra Van car where the relative damping coefficient was $\vartheta_1 = 0.242$: (**a**) curves representing the phase angle as a function of the frequency of the contact force between the tyre and the vibration plate (without the disturbing impact of the inertia of the plate); (**b**) curves representing the phase angle as a function of the frequency of the force measured in the test stand (and including the disturbing impact of the inertia of the vibration plate).

There are visible differences in frequency, which defines the minimum value. However, the phase minimum value is more important for the method. Here, we can see good correspondence. The error of minimum value is 3.8% for Figure 6a and 8.3% for Figure 6b.

3.3. Comparison of the Simulation Results Obtained for the Two Models and the Experimental Test Results

Figure 7 is a juxtaposition of the minimum values of the phase shift angle, obtained as a result of simulation calculations where the linear and non-linear models were used, and results of experimental tests carried out on a prototype diagnostic test stand. The independent variable is the relative suspension damping coefficient ϑ_1 ('Theta1'). It should be remembered that the force Fts_1 of sliding friction in the suspension system is not taken into account in this coefficient. Figure 7a shows the minimum values (Φ_{min} = Fimin) of the phase shift angle for the contact force between the tyre and the vibration plate, and Figure 7b

shows the minimum values (Φ_{mmin} = Fimmin) of this angle for the force measured in the test stand (and including the disturbing impact of the inertia of the vibration plate). Both of these illustrations apply to the rear suspension of the Opel Astra Van car. Figure 8a,b present analogous quantities for the rear suspension of the Opel Agila car.

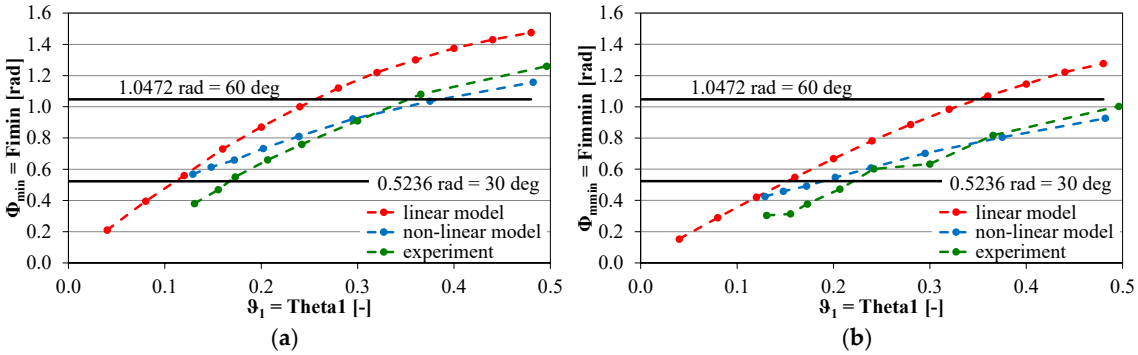

Figure 7. Minimum values of the phase shift angle vs. relative damping coefficient ϑ_1 ('Theta1') for the rear suspension of the Opel Astra Van car: (**a**) Φ_{min} (Fimin) values for the contact force between the tyre and the vibration plate; (**b**) Φ_{mmin} (Fimmin) values for the force measured in the test stand.

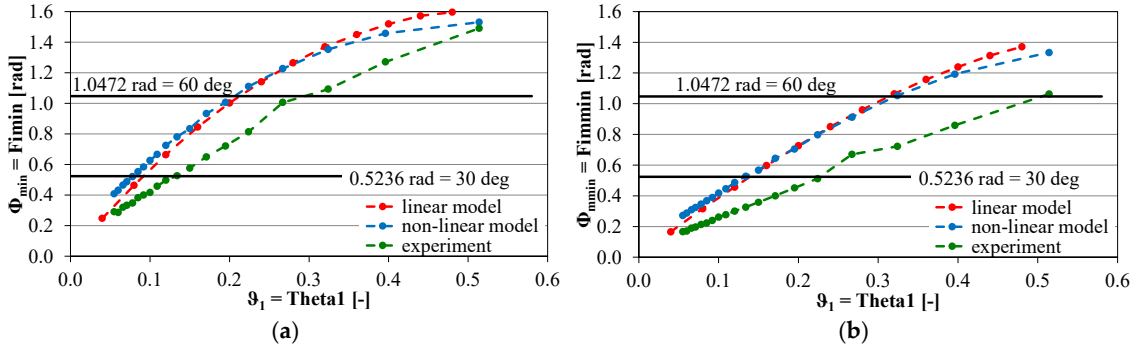

Figure 8. Minimum values of the phase shift angle vs. relative damping coefficient ϑ_1 ('Theta1') for the rear suspension of the Opel Agila car: (**a**) Φ_{min} (Fimin) values for the contact force between the tyre and the vibration plate; (**b**) Φ_{mmin} (Fimmin) values for the force measured in the test stand.

The results of calculations where the linear and non-linear models were used and the results of experiments have a similar qualitative nature. With growing relative suspension damping ϑ_1, the minimum values of the phase angle Φ_{min} (Fimin) and Φ_{mmin} (Fimmin) are increasing almost linearly, too. In quantitative terms, however, they differ considerably from each other. The monotonicity observed, and the noticeable sensitivity to changes in the condition of shock absorbers (measured by the slope of the $\Phi_{min}(\vartheta_1)$ and $\Phi_{mmin}(\vartheta_1)$ characteristic curves) is a crucial and desired feature in diagnostics.

The simulation results obtained for the linear and non-linear models significantly differ from each other in quantitative terms in the case of the Opel Astra Van car (Figure 7) and are close to each other for the Opel Agila car (Figure 8). When the data of the 'quarter-car' models of the two cars are compared with each other (Tables 1 and 2 vs. Tables 3 and 4), significant similarity can be seen. However, a considerable difference is observed as regards the sliding friction force, whose amplitude for the Opel Astra Van suspension system is twice as big as that for the Opel Agila car (see Tables 2 and 4: Ats_1 is equal to 40 N and 20 N, respectively). It should be pointed out here that the equivalent damping adopted in the linear model stems from the assumption of equality of the value of the energy dissipated in the shock absorber in a single cycle. However, the sliding friction is not taken into account in such an assumption. As can be seen, increased friction raises the minimum value of the phase shift angle. This is not in conformity with the widely known thesis (promoted in

theoretical publications, e.g., [40,41]) that friction (or, more precisely, dry friction) has no impact on the phase shift angle between the input and response of a system under analysis.

The quantitative differences between the results of simulations where the linear model was used and the results of experiments are big (although smallest for low relative suspension damping coefficients) in spite of qualitative similarities in the dependences of the minimum phase angle on the relative suspension damping. This indicates the necessity to limit the application of linear models to qualitative analyses only.

What should additionally be recalled here are the general criteria for the assessment of the technical condition of a shock absorber, proposed in publications [16,17] (see also [28]). The acceptable minimum values of the phase shift angle should be higher than 0.52360 rad (30 deg). The suspension systems with "strong" shock absorbers are characterised by the values of this angle exceeding 1.04720 rad (60 deg). In consideration of the results presented in Figures 7 and 8, the minimum value of this angle, i.e., 0.52360 rad (30 deg), corresponds to the relative suspension damping ϑ_1 (Theta1) in the interval 0.1–0.15 (for the assessment based on the contact force between the tyre and the vibration plate). In publication [16] (see also [28]), the very good shock absorbers' condition is described by the minimum phase shift angle values exceeding 1.5708 rad (90 deg).

As an additional problem, we should also mention the significant differences between the values obtained by analysing the contact force F_{dz} between the tyre and the vibration plate (the angle Φ_{min} = Fimin) and the force F_{md} measured (the angle Φ_{mmin} = Fimmin) clearly visible in Figures 7 and 8. This indicates that the correction made to take into account the value of the force of inertia of the vibration plate is very important in both qualitative and quantitative terms. The values determined without the correction are lower, although this is not justified by the condition of the vehicle under examination, defined by the relative suspension damping ϑ_1. This confirms the reasonableness of correcting the force measured in the diagnostic test stand to take into account the force of inertia of the vibration plate, as postulated in publications [16,17,27].

For the non-linear model, relative error (simulation versus real car) is on level 0.4–11.0% (Figure 7), but for very small $\Delta\vartheta$, it reaches values up to 44%. Similar values for Figures 8 and 9 are up to 30%. For the linear model, the relative error reaches 11.8–38% (Figure 8a) and 36–57% (Figure 8b). A similar situation is for Figure 9, an inverted version (prepared for diagnostic purposes) of Figure 8. So, we can say that the non-linear model shows better properties of real cars than linear ones.

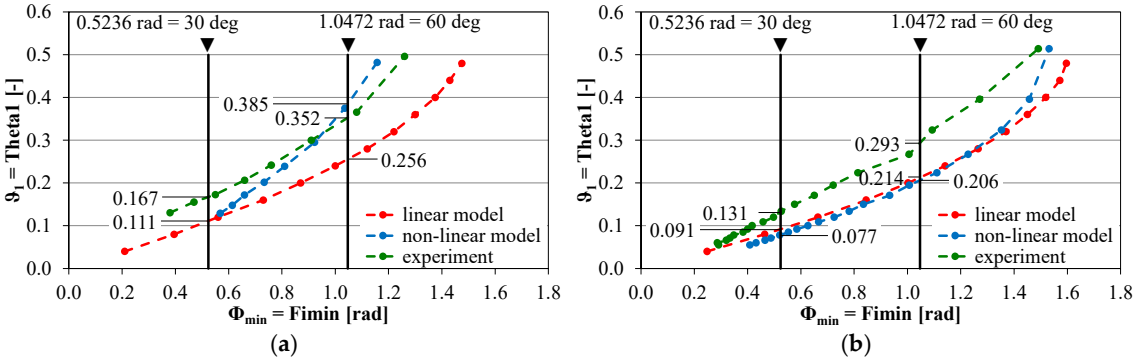

Figure 9. Illustration of the diagnostic assessment of the relative damping ϑ_1 = Theta1 in the vehicle's suspension system based on the minimum values of the phase shift angle Φ_{min} = Fimin for the contact force between the tyre and the vibration plate: (**a**) results of simulation and experimental testing of the rear suspension of the Opel Astra Van car; (**b**) results of simulation and experimental testing of the rear suspension of the Opel Agila car.

Based on the results presented, we can also state that the method presented is very sensitive to suspension friction forces.

3.4. Use of the Obtained Results of Simulation and Experimental Tests in the Assessment of Damping Characteristics of Suspensions of the Vehicles Under Test

The results shown in Figures 7 and 8 were used for the assessment of damping characteristics of suspensions, chiefly shock absorbers, of the vehicles under test. For this objective to be attained, the test results (i.e., the set of values of the functions under analysis) in the form of the minimum values of the phase shift angle Φ_{min} (Fimin) defined the domain of the analysis and the values of the relative damping ϑ_1 ('Theta1') in the suspension system under test were to be found. This means an inversion of the dependencies that are graphically described by Figures 7a and 8a, i.e., only those that are related to the contact force between the tyre and the vibration plate or, in other words, those where the recommended correction taking into account the force of inertia of the vibration plate is applied. In consequence, Figures 9a and 9b have been plotted for the suspension systems of the Opel Astra Van and Opel Agila cars, respectively.

Example results of the assessment of the relative damping coefficient ϑ_1 = Theta1 of the car suspension system for two example minimum values of the phase shift angle Φ_{min} = Fimin (Φ_{min} = 0.5236 rad = 30 deg and Φ_{min} = 1.0472 rad = 60 deg) have been marked in Figure 9 and juxtaposed in Table 6.

Table 6. Example results of the assessment of the relative damping coefficient ϑ_1 = Theta1 in the rear suspension systems of the Opel Astra Van and Opel Agila cars for two minimum values of the phase shift angle Φ_{min} = Fimin.

	ϑ_1 (Linear Model)		**ϑ_1 (Non-Linear Model)**		**ϑ_1 (Experiment)**	
	Opel Astra	**Opel Agila**	**Opel Astra**	**Opel Agila**	**Opel Astra**	**Opel Agila**
Φ_{min} = 0.5236 rad = 30 deg	0.111	0.091	–	0.077	0.167	0.131
Φ_{min} = 1.0472 rad = 60 deg	0.256	0.214	0.385	0.206	0.352	0.293

The linear model lowers the values ϑ_1 because it merely represents the viscous damping of the shock absorber, and in a considerably simplified way at that (see [43]). The results of experiments and calculations carried out for the non-linear model (but for relatively high forces of the sliding friction in the suspension system, e.g., those for the Opel Astra Van car) are the most optimistic. This is due to the impact of the sliding friction as described herein. In the experimental and simulation tests carried out for the non-linear model, the assessment covers the overall damping characteristics of the suspension system instead of those of the shock absorber alone. It can be seen from the above that friction in the suspension system is an important disturbing element in the assessment of shock absorber conditions, as signalled previously in publications [3,5,25].

4. Discussion

The calculations and experimental tests make it possible to formulate general qualitative and quantitative conclusions.

Distinct differences can be seen between the minimum phase angle values obtained by analysing the contact force between the tyre and the vibration plate and the values determined from the curve representing the force measured in the test stand. The correction made to take into account the value of the force of inertia of the vibration plate is very important in both qualitative and quantitative terms. The results (i.e., the measured minimum phase angle value) where the said correction has not been made suggest (for both the simulation models used and for the experiment) higher values of the relative damping in the suspension system, although this is not justified by the condition of the vehicle under examination, especially of the shock absorbers (ϑ_1 represents the damping of vehicle's shock absorbers).

The minimum values of the phase shift angle are increasing almost linearly with growing suspension damping. A statement may be made that it is easy to notice the monotonicity of changes in this diagnostic parameter and its high sensitivity to changes

in the diagnosed quantity that represents the relative damping in the suspension system under examination. This is a crucial and desired feature in diagnostics, which facilitates the determining of the sought value of the relative damping coefficient.

Nevertheless, the presented results of simulation and experimental tests confirm that the phase angle method makes it possible to assess, above all, the general damping properties of the suspension system rather than the condition of a shock absorber alone. The friction in the suspension system is here an important disturbing factor.

So, the phase angle method is qualitatively and quantitatively effective in determining the damping properties of a car suspension; however (similarly to the EUSAMA method), it is very sensitive to suspension friction forces.

Author Contributions: Conceptualisation, Z.L. and P.Z.; methodology, Z.L., J.D. and P.Z.; software, J.D., Z.L. and P.Z.; validation, J.D. and P.Z.; formal analysis, Z.L., J.D. and P.Z.; investigation, Z.L., P.Z.; resources, Z.L., P.Z. and J.D.; data curation, Z.L., P.Z. and J.D.; writing—original draft preparation, Z.L., J.D. and P.Z.; writing—review and editing, J.D. and P.Z.; visualisation, J.D. and P.Z.; supervision, Z.L.; project administration, Z.L. and P.Z.; funding acquisition, Z.L. All authors have read and agreed to the published version of the manuscript.

Funding: The part of research for the article was financed by WUT project no. 501210101325 sposored by UNIMETAL Sp. z o.o. Złotów, Poland. This paper was also co-financed under the research grant of the Warsaw University of Technology, supporting the scientific activity in the discipline of Civil Engineering, Geodesy and Transport.

Institutional Review Board Statement: Not applicable.

Informed Consent Statement: Not applicable.

Data Availability Statement: All data are included in the manuscript.

Acknowledgments: The authors of this paper would like to thank UNIMETAL Sp. z o.o. Zlotów, Poland for their cooperation. The test results presented in this paper were obtained using, among other things, a prototype TUZ-1/E device from this manufacturer.

Conflicts of Interest: The authors declare that this study received funding from UNIMETAL Sp. z o.o. Złotów, Poland. The funder was not involved in the study design, collection, analysis, interpretation of data, the writing of this article or the decision to submit it for publication.

References

1. Calvo, J.A.; Díaz, V.; San Román, J.L.; García-Pozuelo, D. Influence of shock absorber wearing on vehicle brake performance. *Int. J. Automot. Technol.* **2008**, *9*, 467–472. [CrossRef]
2. Calvo, J.A.; López-Boada, B.; San Román, J.L.; Gauchía, A. Influence of a shock absorber model on vehicle dynamic simulation. *Proc. Inst. Mech. Eng. Part D J. Automob. Eng.* **2009**, *223*, 189–202. [CrossRef]
3. Guzek, M.; Zdanowicz, P. Diagnostics of the On-Vehicle Shock Absorber Testing. *Communications* **2021**, *23*, B178–B186. [CrossRef]
4. Lozia, Z. The use of a linear quarter-car model to optimize the damping in a passive automotive suspension system—A follow-on from many authors' works of the recent 40 years. *Arch. Automot. Eng.* **2016**, *71*, 33–65. [CrossRef]
5. Zdanowicz, P. Comparative assessment of vertical vibrations of a vehicle on the road and during the EUSAMA test. *IOP Conf. Ser. Mater. Sci. Eng.* **2018**, *421*, 022045. [CrossRef]
6. Szczypinski-Sala, W.; Kot, A.; Hankus, M. The Evaluation of Vehicle Vibrations Excited with a Test Plate during Technical Inspection of Vehicle Suspension. *Appl. Sci.* **2023**, *13*, 11. [CrossRef]
7. Buzzi, C. System for Measuring the Damping Coefficient of Vehicle-Mounted Shock Absorbers. European Patent EP0647843A2, 12 April 1995.
8. Calvo, J.A.; Diaz, V.; San Román, J.L. Establishing inspection criteria to verify the dynamic behaviour of the vehicle suspension system by a platform vibrating test bench. *Int. J. Veh. Des.* **2005**, *38*, 290–306. [CrossRef]
9. Calvo, J.A.; San Román, J.L.; Alvarez-Caldas, C. Procedure to verify the suspension system on periodical motor vehicle inspection. *Int. J. Veh. Des.* **2013**, *63*, 1–17. [CrossRef]
10. Gardulski, J. Metody badań amortyzatorów samochodów osobowych (Testing methods for vehicle shock absorbers). *Diagnostyka* **2009**, *3*, 93–100.
11. Klapka, M.; Mazůrek, I.; Kubìk, M.; Macháček, O. Reinvention of the EUSAMA diagnostic methodology. *Int. J. Veh. Des.* **2017**, *74*, 304–318. [CrossRef]

12. Klapka, M.; Mazůrek, I.; Macháček, O.; Kubìk, M. Twilight of the EUSAMA diagnostic methodology. *Meccanica* **2017**, *52*, 2023–2034. [CrossRef]
13. Knestel, A.; Küchle, J. Procedure and Device for Determining a Measure of the Vibration Absorption of Vehicles. European Patent EP1564538B1, 11 February 2005.
14. Mazůrek, I.; Klapka, M. Method of Measuring Damping Ratio of Unsprung Mass of Half Axles of Passenger Cars Using a Suspension Testing Rig Without Disassembling. European Patent EP3193152A1, 15 January 2016.
15. Szymański, G.M.; Jósko, M.; Tomaszewski, F.; Filipiak, R. Application of time–frequency analysis to the evaluation of the condtion of car suspension. *Mech. Syst. Signal Process.* **2015**, *58–59*, 298–307. [CrossRef]
16. Tsymberov, A. An improved non-intrusive automotive suspension testing apparatus with means to determine the condition of the dampers. *SAE Tech. Pap.* **1996**. [CrossRef]
17. Tsymberov, A. Suspension Tester and Method. U.S. Patent 5,369,974, 6 December 1994.
18. Hryciów, Z.; Rybak, P.; Gieleta, R. The influence of temperature on the damping characteristic of hydraulic shock absorbers. *Eksploat. I Niezawodn.-Maint. Reliab.* **2021**, *23*, 346–351. [CrossRef]
19. Hryciów, Z. An Investigation of the Influence of Temperature and Technical Condition on the Hydraulic Shock Absorber Characteristics. *Appl. Sci.* **2022**, *12*, 12765. [CrossRef]
20. Pikunas, A.; Spruogis, B. Research of the efficiency of use of shock absorbers with controlled dissipative force in motor cars. *Eksploat. I Niezawodn.-Maint. Reliab.* **2002**, *1*, 3–6.
21. Hryciów, Z.; Krasoń, W.; Wysocki, J. Evaluation of the influence of friction in a multi-leaf spring on the working conditions of a truck driver. *Eksploat. I Niezawodn.-Maint. Reliab.* **2021**, *23*, 422–429. [CrossRef]
22. Dukalski, P.; Będkowski, B.; Parczewski, K.; Wnęk, H.; Urbaś, A.; Augustynek, K. Dynamics of the vehicle rear suspension system with electric motors mounted in wheels. *Eksploat. I Niezawodn.-Maint. Reliab.* **2019**, *21*, 125–136. [CrossRef]
23. Arbeláez-Toro, J.J.; Rodriguez-Ledesma, C.M.; Hincapié-Zuluaga, D.A.; Torres-Lopez, E.A. Adherence Evaluation of a MacPherson Suspension under EuSAMA Norm in a Mathematical Model and one Multibody. *TecnoLógicas* **2013**, 757–768. [CrossRef]
24. Balsarotti, S.; Bradley, W. Experimental evaluation of a non-intrusive automotive suspension testing apparatus. *SAE Tech. Pap. Ser.* **2000**. [CrossRef]
25. Guzek, M.; Zdanowicz, P. Effects of Using Various Methods for Car Shock Absorbers Diagnostic Tests. *Arch. Automot. Eng.* **2020**, *88*, 99–108. [CrossRef]
26. Lozia, Z. Assessment of the usability of the EUSAMA and the phase angle method in examining the condition of shock absorbers installed in a vehicle. *WUT J. Transp. Eng.* **2021**, *132*, 61–79. [CrossRef]
27. Lozia, Z.; Zdanowicz, P. Simulation assessment of the impact of inertia of the vibration plate of a diagnostic suspension tester on results of the EUSAMA test of shock absorbers mounted in a vehicle. *IOP Conf. Ser. Mater. Sci. Eng.* **2018**, *421*, 022018. [CrossRef]
28. Martinod, R.M.; Betancur, G.R.; Mesa, J.F.; Benavides, O.M.; Castañeda, L.F. Analysis of the procedure for suspension evaluation of civil armoured vehicles: Reliability and safety driving criteria. *Int. J. Veh. Saf.* **2013**, *6*, 254–264. [CrossRef]
29. Šarkan, B.; Vrábel, J.; Skrúcaný, T.; Ševčík, M. Methods of assessing the technical condition of automotive shock absorbers in the road vehicles operation. *Int. Sci. J. "Mach. Technol. Mater."* **2015**, *9*, 52–54.
30. Stańczyk, T.L.; Jurecki, R. Analiza porównawcza metod badania amortyzatorów hydraulicznych (Comparative analysis of testing methods of hydraulic shock absorbers). *Zeszyty Naukowe Instytutu Pojazdów PW (Proc. Inst. Veh. Wars. Univ. Technol.)* **2014**, *4*, 25–45.
31. Toma, M.; Andreescu, C.; Stan, C. Influence of tire inflation pressure on the results of diagnosing brakes and suspension. *Procedia Manuf.* **2018**, *22*, 121–128. [CrossRef]
32. Zuska, A.; Jackowski, J. Influence of Changes in Stiffness and Damping of Tyre Wheels on the Outcome of the Condition Assessment of Motor Vehicle Shock Absorbers. *Energies* **2023**, *16*, 3876. [CrossRef]
33. Podosek, K.; Jaśkiewicz, M.; Zuska, A. Testing the relationship between the technical condition of motorcycle shock absorbers determined on the diagnostic line and their characteristics. *Open Eng.* **2023**, *13*, 20220435. [CrossRef]
34. Lozia, Z. Application of modelling and simulation to evaluate the theta method used in diagnostics of automotive shock absorbers. *Arch. Automot. Eng.* **2022**, *96*, 5–30. [CrossRef]
35. Lozia, Z.; Zdanowicz, P. Simulation assessment of the half-power bandwidth method in testing shock absorbers. *Open Eng.* **2021**, *11*, 120–129. [CrossRef]
36. Buekenhoudt, P. GOCA. Minimum phase shift. In Proceedings of the CITA 2011 Conference and 15th General Assembly, Berlin, Germany, 4–6 May 2011.
37. Stańczyk, T.L. Analysis of the possibilities of using the phase angle as a diagnostic parameter in shock absorber examinations. *Arch. Transp.* **2004**, *16*, 33–50.
38. Dixon, J.C. *The Shock Absorber Handbook*, 2nd ed.; SAE International: Warrendale, PA, USA; John Wiley & Sons Ltd.: Hoboken, NJ, USA, 2007.
39. Dukkipati, R.V.; Pang, J.; Qatu, M.S.; Sheng, G.; Shuguang, Z. *Road Vehicle Dynamics*; SAE International: Warrendale, PA, USA, 2008.
40. Rao, S.S. *Mechanical Vibrations*, 5th ed.; Prentice Hall—PEARSON: Hoboken, NJ, USA, 2010.
41. Rill, G.; Castro, A.A. Road Vehicle Dynamics. In *Fundamentals and Modeling with MATLAB*, 2nd ed.; CRC Press: Boca Raton, FL, USA; Taylor&Francis Group: Abingdon, UK, 2020.

42. All About Öhlins Steering Dampers. Available online: https://www.ohlinscommunity.com/okc-steering-damper-sg (accessed on 3 October 2024).
43. Skačkauskas, P.; Žuraulis, V.; Vadluga, V.; Nagurnas, S. Development and verification of a shock absorber and its shim valve model based on the force method principles. *Eksploat. I Niezawodn.-Maint. Reliab.* **2017**, *19*, 126–133. [CrossRef]